Journal of Ultrafine Grained and Nanostructured Materials
https://jufgnsm.ut.ac.ir
Vol. 56, No.1, June 2023, pp. 121-128
Print ISSN: 2423-6845 Online ISSN: 2423-6837
DOI: 10.22059/jufgnsm.2023.01.12

Luminescent properties of graphene quantum dots (GQDs) functionalized with $L_{Cysteine}$

Ali Moeini, Hossein Anabestani, Hamid Reza Madaah Hosseini, Adrine Malek Khachatourian**

Department of Materials Science and Engineering, Sharif University of Technology, Azadi Avenue, P.O. Box 11155-9466, Tehran, Iran.

Recieved: 2 June 2023; Accepted: 28 June 2023

**Corresponding author email: madaah@sharif.edu, khachatourian@sharif.edu*

ABSTRACT

Graphene quantum dots (GQDs) are one of the most uprising nanomaterials that have been used in biomedical applications because of their interesting luminescent properties. This work presents a facile way to attach the $L_{Cysteine}$ onto the surface of GQDs, which enhances the applicability of the final molecules in biomedical applications. Furthermore, the luminescent properties of synthesized GQDs and GQDs-$L_{Cysteine}$ have been investigated with different methods. The obtained GQDs-$L_{Cysteine}$ show a red shift in PL results with an increase in $L_{Cysteine}$ content compared to GQDs. According to the results, this platform has the potential to be used in many biological applications, such as bio-imaging and bio-labeling.

Keywords: *Graphene quantum dots ; $L_{Cysteine}$; Optical properties ; Luminescent ; Biomedical applications*

1. Introduction

Among the various complicated and lethal illnesses that are still usually treatable, cancer is one of the major causes of mortality. When cancer cells have not gone far in the body, surgery can successfully treat the disease in its early stages. However, because of its invasive nature, surgery is often not recommended in the latter stages of cancer [1], [2]. Early detection of the disease in its early stages can slow its progression and boost the probability of treatment. Accordingly, many different types of materials have been developed in order to improve the contrast in a variety of imaging methods, such as magnetic resonance imaging (MRI) [3]–[5], fluorescence imaging (FI) [6]–[8], or in dual/multi-imaging methods [9]–[11].

Graphene quantum dots (GQDs) have attracted magnificent research interest due to their particular aspects, such as photoluminescence (PL) properties, low cytotoxicity, easy modification, and resistance to photobleaching, which are directly associated with quantum confinement and chemical functionalization [12]. Because of these properties, they are suitable for bioimaging, sensors, catalysis, and photovoltaic devices [13], [14].

GQDs synthesis methods are mainly classified into two main strategies: top-down and bottom-up. In top-down methods, GQDs are prepared from a large carbon structure by several processes such as acid oxidation, electrochemical, oxidation, and thermal decomposition. In top-down methods, carbonaceous materials are dismantled by physical, chemical, or electrochemical techniques to produce GQDs. These materials include carbon nanotubes (CNT), graphene oxide (GO), graphene, and graphite powder. However, in bottom-up approaches, such as solution chemistry, solvothermal synthesis, and microwave-assisted

approaches, GQDs are fabricated from molecular precursors under particular reaction conditions [12]. In order to carburize small organic molecules, bottom-up techniques involve the field of chemical synthesis. This includes employing pyrolysis in addition to specific chemical processes. In order to start the process, these approaches require the use of severe conditions, such as combustion, thermal treatment, chemical carbonization, and alkali- or acid-assisted oxidation processes [15].

The PL spectrum of GQD is the most interesting property of this material. In relation to the synthesis techniques, various particle sizes will create unique colors [16], such as blue, green, yellow, and red, when they are excited by UV light [17]. These colors will be produced regardless of the method of synthesis. The luminescent properties of GQDs are mainly driven by the quantum size effect, zig-zag sites, and defect effect [18]. Generally, quantum confinement effects and zig-zag sites are classified as intrinsic scattering sites, while structural defects are categorized as defect state emissions. Furthermore, intrinsic sites can be induced by the recombination of electron-hole pairs [19]. Different factors can affect the luminescent properties of GQDs in distinct synthesis methods. These factors mainly include particle size [16], the wavelength of excitation [20], pH [21], the polarization of solvent [22], surface oxidation degree [23], doping atoms [24], and functionalized molecules [25].

The PL mechanism of GQD is ascribed to both intrinsic, defect, and extrinsic emission states. From the point of view of intrinsic states, chemical doping could be an efficient method for tuning electronic properties [26]. For example, H. Tetsuka et al. [24] investigated the effect of direct nitrogen (N) substitution in the GQDs lattice. They showed that because of the high electronic affinity of N atoms, this substitution would induce the modulation of chemical and electronic characteristics of GQDs and thus alter the GQDs to indicate a blue shift in the PL emission. However, heteroatom doping into the graphene lattice would disrupt the hybridization of basal C atoms, and there is no control over how it would impact the optical properties [27].

Another way to tune the luminescent properties of GQDs is to use molecules with strong electron-donating or accepting abilities to modify the surface of GQDs chemically. For instance, primary amines could significantly affect the electronic properties of GQDs via the selective and quantitative functionalization of amines onto the surface of tunable GQDs [24]. To explain the mechanism of PL in the functionalized GQDs, the importance of strong orbital interactions between primary amines should be noted. A degenerate highest occupied molecular orbital (HOMO) orbital was raised to a higher energy level, narrowing the band gap [28].

The surface modification not only enhances the quantum yield and luminescent efficiency of GQDs but also provides an important intermediate for the resultant functionalization [29]. $L_{Cysteine}$, a semi-essential amino acid biosynthesized by organisms with the formula [$HO_2CCH(NH_2)CH_2SH$], has three active functional groups, including thiol (-SH), carboxylic (-COOH), and amino (-NH_2), is biocompatible and inexpensive [30], [31]. Hence, $L_{Cysteine}$ with appropriate binding capacities could prevent MNPs from oxidizing, transform them into significantly soluble and stable particles in organic solutions, and improve the goods' biocompatibility [3], [32]. Also, $L_{Cysteine}$ significantly reduces the toxicity of metal nanoparticles in clinical applications [33].

In this research, GQDs were fabricated through the pyrolysis of citric acid until their color turned orange. Then they were functionalized with $L_{Cysteine}$ via reflux. Here, the role of $L_{Cysteine}$ is to design a graphene structure with a novel modification method and tune its electronic features by introducing primary amines onto the surface of GQDs. Moreover, this modification could be applied to modify the PL and luminescent characteristics of GQDs to be appropriate for biomedical applications.

2. Materials and methods

2.1. Materials

All chemical reactants and reagents used in this research were of analytical grade and were used as received without further purification. Sodium hydroxide (NaOH, Merck, CAS number: 1310-73-2), hydrochloric acid (HCl, Merck, CAS number: 7647-01-0), ammonia solution 25% (NH_4OH, Merck, CAS number: 7664-41-7), citric acid ($C_6H_8O_7$, Merck, CAS number: 77-92-9), and $L_{Cysteine}$ ($C_3H_7NO_2S$, BioChem, CAS number: 52-90-4) were used as the synthesizing reagents.

2.2. Synthesis of GQDs

GQDs were fabricated by heating citric acid at 200 °C [10]. In this method (Fig. 1a), 2 g of citric acid (CA) was added to the container and then heated for 30 minutes on the heater. Meanwhile,

100 g NaOH in 100 ml of deionized (DI) water was added to this mixture. The pH of the prepared solution was 12, then a few drops of 37% HCl were added to the solution to change the pH to 7. Finally, the GQDs were poured into a dark bottle and stored in the refrigerator to protect them from sunlight.

2.3. Synthesis of GQDs-$L_{Cysteine}$

In this regard, 10 ml of the as-synthesized GQDs were poured into the balloon. Afterward, 0.1, 0.2, 0.3, 0.4, and 0.5 wt.% of $L_{Cysteine}$ powder were solved in 50 ml of DI water, then mixed with GQD solution at room temperature (25 °C). Next, each balloon was refluxed at 80 °C for 24 h. Obtained solutions were checked under the UV lamp for their luminescent measurement. The schematic of the synthesis method is illustrated in Fig. 1b.

2.4. Materials characterizations

The FT-IR spectra were acquired in transmission mode with a Thermo Nicolet AVATAR 360 FT-IR spectrometer in the 1000-4000 cm^{-1} spectral range at ambient temperature. Prior to fabricating the KBr particle for the FT-IR analysis, the samples were dried out at 50 °C. Using a JENWAY 6705 UV-Vis spectrophotometer, the optical characteristics of synthesized particles were measured. Using a Raman spectrometer (Teksan company, Takram P50COR10, laser wavelength=532 nm), particulate Raman spectra were recorded. In addition, the Cary Eclipse photoluminescence spectrometer was utilized to measure the PL spectra of samples.

3. Results and Discussion

GQDs were successfully synthesized through facile CA carbonization to convert them to dots with different functional groups on their basal plane and edges. To verify the synthesis of GQDs, based on the literature [34], during the CA pyrolysis, the color of the solution should turn orange, which means the degree of CA carbonization is in the range and proves incomplete carbonization and GQDs fabrication. In addition, high oxygen-containing functional groups and active chemical groups modify the surface chemistry of GQDs and tune their optical properties. $L_{Cysteine}$ is an organic molecule with nitrogen-containing functionalities that can affect the abovementioned features. In order to confirm the functionalization of $L_{Cysteine}$ onto GQDs and also evaluate the luminescent properties of GQDs and modified GQDs, different characterization methods were used.

3.1. FTIR analysis

Fig. 2 represents the FT-IR spectra of GQD and GQD-$L_{Cysteine}$, which were applied to investigate the functional groups on the GQDs. In this spectrum, a wide absorptive band of 3253 cm^{-1} referred to stretching vibrations of O-H groups. The bands in 1530 cm^{-1} and 1336 cm^{-1} are, respectively, proofs for the presence of C=C and C-O groups on GQDs [35].

During the synthesis of GQD-$L_{Cysteine}$ with different ratios of 1, 2, 3, and 4 wt.% $L_{Cysteine}$ in the reflux stage, in situ, chemical bonding between

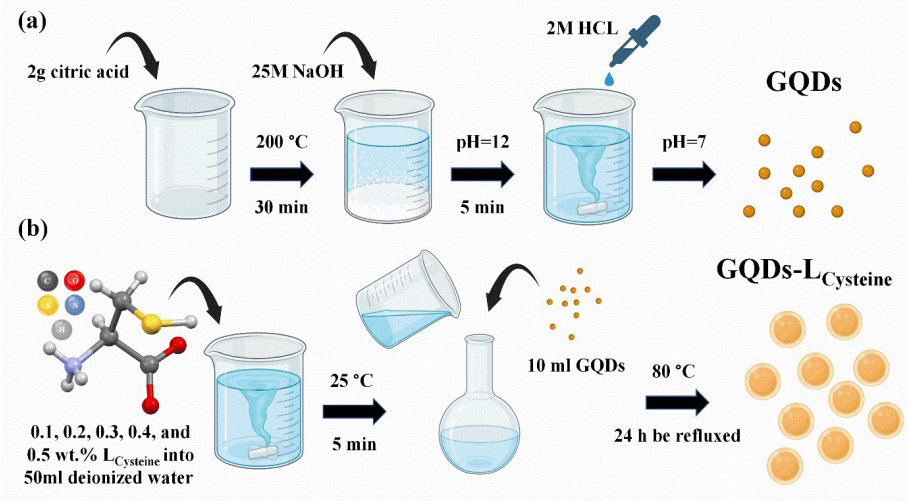

Fig. 1- Schematic illustration of the synthetic process of a) GQDs by hydrothermal method and b) $L_{Cysteine}$ functionalized GQDs nanocomposites. This figure was created using BioRender (https://biorender.com).

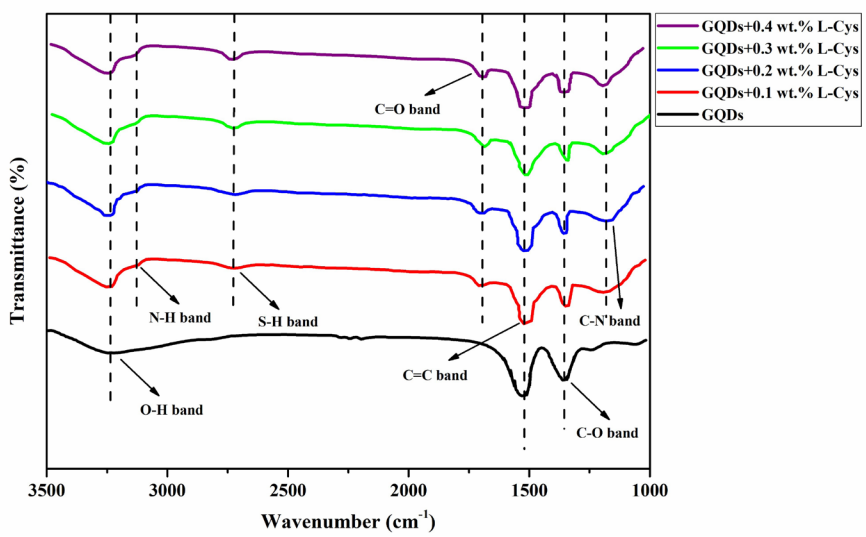

Fig. 2- FTIR spectra of x wt.% $L_{Cysteine}$-GQDs nanocomposites (x=0.1, 0.2, 0.3, and 0.4).

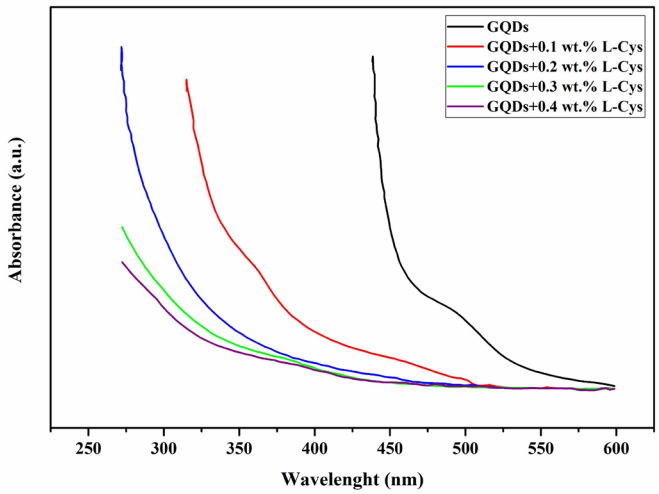

Fig. 3- UV–Vis absorption spectra of x wt.% $L_{Cysteine}$-GQDs nanocomposites (x=0.1, 0.2, 0.3, and 0.4).

carboxyl groups and fresh amine functions occurred adequately. The bands in 1693 cm^{-1} and 1194 cm^{-1} are associated with the presence of C=O and C-N groups on the GQDs. The absorptive band in 3123 cm^{-1} is related to the stretching vibrations of N-H, which strongly validates the presence of nitrogen-containing groups on GQDs. Also, the band of 2722 cm^{-1} could be dependent on the stretching vibrations of S-H as a sign of the remaining S-H group during functionalization and proof for the fact that the procedure of connection merely happened via -NH_2 groups [36]. While with increasing amounts of $L_{Cysteine}$ (0.1 to 0.4 wt.%), picks of N-H and S-H became sharper.

3.2. UV-Vis spectroscopy

Fig. 3 represents the UV-Vis absorption spectrum of the pristine GQD and the compounds with 0.1, 0.2, 0.3, and 0.4 wt.% $L_{Cysteine}$. GQDs exhibit a peak at 321 nm, and a shoulder at 452 nm due to the electron transitions from π to π* of C=C and n to π* of C=O bonds. It has been shown that the degree of carbonization strongly affects the size, quality, and luminescent properties of the resultant species. Furthermore, CA only shows a UV absorption peak below 250 nm, but the absorption peak of GQDs is a distinct band at 362 nm with narrow full width at half maximum of 66 nm. This confirms that the sp^2 clusters included in GQDs

should be uniform in size.

On the one hand, the UV-Vis spectrum of GQDs with different amounts of $L_{Cysteine}$ indicates an obvious shift of the two peaks to 331 nm and 503 nm after the functionalization of GQDs with $L_{Cysteine}$. The absorption peak position decreased in the 200-700 nm region compared to GQDs. This issue reveals that electronic conjugation was disrupted because of the presence of the $L_{Cysteine}$ molecules on the surface of GQDs [37]. The noteworthy point is that with the increase in the amount of $L_{Cysteine}$ (0.1 to 0.4 wt.%), the absorption peak moves to lower wavelengths.

3.3. PL spectroscopy

Fig. 4 depicts the PL spectrum of the GQDs at room temperature and excited at 325 nm. As was expected, a strong blue emission band can be seen at 460 nm in the abovementioned conditions. As known, graphene is a zero-band gap material, and observing its optical properties is strongly unlikely. However, GQDs contain many sp^2 structures and oxygen groups that play important roles in fluorescent emissions [38].

In the comparison between the PL spectrum of GQDs and GQDs functionalized with different ratios of $L_{Cysteine}$, it has been found that by increasing the percentage of $L_{Cysteine}$ from 0.1 to 0.4 wt.%, the emission band also shifts from 460 nm to 501 nm, respectively, to reach higher wavelengths and experience a redshift. This implication shows the functionalization of GQDs with $L_{Cysteine}$, confirming the point that GQDs reveal blue fluorescence while GQD-$L_{Cysteine}$ emits green light under a UV lamp. The redshift of the PL peak has been seen in GQDs functionalized with NH_3 and PEG-diamine and is ascribed to the electron transfer from amino groups to the GQDs, narrowing the band gap. Another justification for this change could be the higher interaction between the amine groups and the π- π systems on the basal domains, leading to a lift of functionalized GQDs' degenerative HOMO orbitals to higher energy [39]. The other fact that could be mentioned is that because of the shift in the PL intensity peak, the GQDs-$L_{Cysteine}$ has a much more powerful PL for each λ_{ex} longer than 450 nm with the corresponding emission wavelength longer than 600 nm. On the other hand, GQDs-$L_{Cysteine}$ has a stronger PL than pristine species, as they are excited by most parts of the visible light. Thus, this luminescent property is truly suitable for bio-imaging applications due to the sensitivity of bio-species to damage from the intense excitation of the blue section of the visible light region.

3.4. Raman spectroscopy

Raman spectroscopy is used to specify more details about the structure of GQDs. The investigation of spectra shows that there are two main peaks, especially related to carbon-based materials, the D band and the G band, which appear as characteristics for GQDs. The D band is

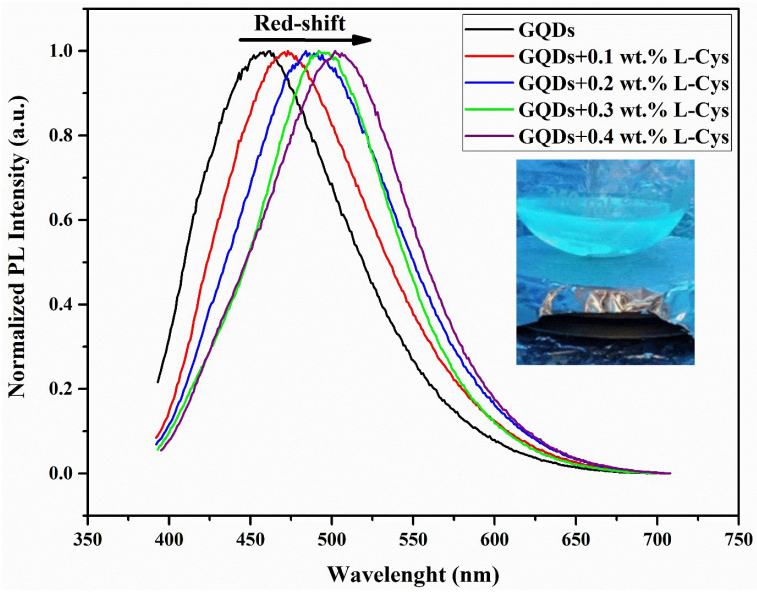

Fig. 4- PL spectra of x wt.% $L_{Cysteine}$-GQDs nanocomposites (x=0.1, 0.2, 0.3, and 0.4).

Table 1- Properties of D and G bands of x wt.% $L_{Cysteine}$-GQDs nanocomposites (x=0.1, 0.2, 0.3, and 0.4)

	I (D_{band})	I (G_{band})	ID/IG
GQDs	0.26	0.24	1.08
GQDs+0.1 wt.% L-Cys	0.48	0.42	1.14
GQDs+0.2 wt.% L-Cys	0.43	0.36	1.19
GQDs+0.3 wt.% L-Cys	0.38	0.31	1.22
GQDs+0.4 wt.% L-Cys	0.35	0.27	1.29

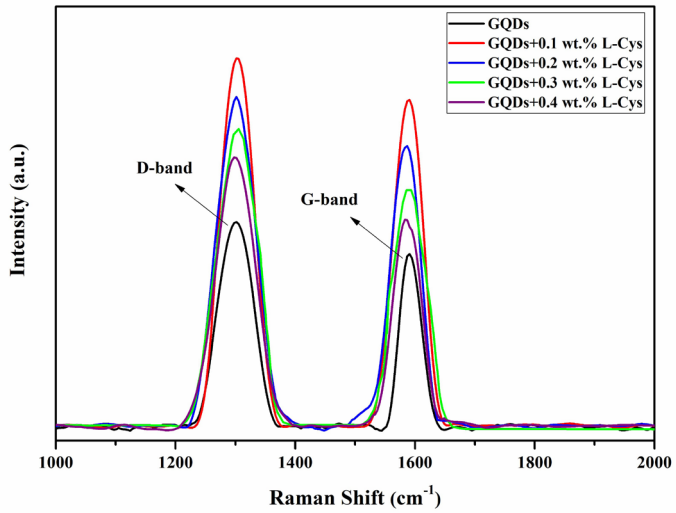

Fig. 5- Raman scattering spectra of x wt.% $L_{Cysteine}$-GQDs nanocomposites (x=0.1, 0.2, 0.3, and 0.4).

a demonstrator for the site of defects and disorders, mostly at the edges, which illustrates the structural defects in the lattice. On the other side, the G band is generally associated with the sp^2 carbon atoms in the hexagonal lattice of 2D clusters of graphene [40], [41]. As shown in Fig. 5, the typical D and G bands of GO, located at 1301 cm^{-1} and 1591 cm^{-1}, respectively, were detected.

On the basis of the study that has been done on the spectra of each compound and considering Fig. 5 and Table. 1, it is evident that by increasing the amount of $L_{Cysteine}$, the intensity of ID/IG grows. This phenomenon could be related to the decrease in the mean size of basal sp^2 nanographene crystallites. Also, this might result in an increase in disorder in the graphene layers. This means that $L_{Cysteine}$ gradually enhances the disordered structure of the GQDs. Considering both pristine GQDs and GQDs-$L_{Cysteine}$, there was a redshift observed for both G and D peaks. These shifts could be attributed to the functionalization of $L_{Cysteine}$ on the surface of the GQDs [36]. Moreover, the ID/IG amount is higher than GQDs for GQDs-$L_{Cysteine}$, indicating the high crystallinity for both groups.

4. Conclusion

In conclusion, the synthesis of $L_{cysteine}$-GQDs by a straightforward and uncomplicated process was demonstrated. This process involves the carbonization of CA and the functionalization of $L_{cysteine}$ via a hydrothermal reaction. Their luminescent properties were studied through different types of prevalent spectroscopies in this field. In this regard, Raman, FTIR, UV-Vis, and PL spectroscopy were applied to evaluate them. One of the notable results is the appearance of a red shift in the PL characterization with an increase in the value of $L_{Cysteine}$ on GQDs. These $L_{cysteine}$-GQD nanocomposites display good potential for biomedical applications via their luminescent properties, such as bio-imaging and bio-labeling.

References

1. Dabbagh Moghaddam F, Akbarzadeh I, Marzbankia E, Farid M, khaledi L, Reihani AH, et al. Delivery of melittin-loaded niosomes for breast cancer treatment: an in vitro and in vivo evaluation of anti-cancer effect. Cancer Nanotechnology. 2021;12(1).
2. A. Moeini, T. Hassanzadeh Chinijani, A. Malek Khachatourian, M. Vinicius Lia Fook, F. Baino, and M. Montazerian, "A critical review of bioactive glasses and glass–ceramics in cancer therapy," Int. J. Appl. Glas. Sci., vol. 14, no. 1, pp. 69–87, 2023.

3. Ahmadi R, Malek M, Hosseini HRM, Shokrgozar MA, Oghabian MA, Masoudi A, et al. Ultrasonic-assisted synthesis of magnetite based MRI contrast agent using cysteine as the biocapping coating. Materials Chemistry and Physics. 2011;131(1-2):170-7.
4. Masoudi A, Madaah Hosseini HR, Shokrgozar MA, Ahmadi R, Oghabian MA. The effect of poly(ethylene glycol) coating on colloidal stability of superparamagnetic iron oxide nanoparticles as potential MRI contrast agent. International Journal of Pharmaceutics. 2012;433(1-2):129-41.
5. Vahdatkhah P, Madaah Hosseini HR, Khodaei A, Montazerabadi AR, Irajirad R, Oghabian MA, et al. Rapid microwave-assisted synthesis of PVP-coated ultrasmall gadolinium oxide nanoparticles for magnetic resonance imaging. Chemical Physics. 2015;453-454:35-41.
6. Fu Y, Jang M-S, Wu T, Lee JH, Li Y, Lee DS, et al. Multifunctional hyaluronic acid-mediated quantum dots for targeted intracellular protein delivery and real-time fluorescence imaging. Carbohydrate Polymers. 2019;224:115174.
7. Vibhute A, Nille O, Kolekar G, Rohiwal S, Patil S, Lee S, et al. Fluorescent Carbon Quantum Dots Functionalized by Poly L-Lysine: Efficient Material for Antibacterial, Bioimaging and Antiangiogenesis Applications. Journal of Fluorescence. 2022;32(5):1789-800.
8. Yang M, Jin H, Gui R. Ag+-doped boron quantum dots with enhanced stability and fluorescence enabling versatile practicality in visual detection, sensing, imaging and photocatalytic degradation. Journal of Colloid and Interface Science. 2023;639:49-58.
9. Sahebalzamani H, Mehrani K, Hosseini HRM, Zare K. Effect of Synthesis Temperature of Magnetic–Fluorescent Nanoparticles on Properties and Cellular Imaging. Journal of Inorganic and Organometallic Polymers and Materials. 2020;30(11):4597-605.
10. Alaghmandfard A, Madaah Hosseini HR. A facile, two-step synthesis and characterization of Fe (3) O (4) -L (Cysteine) -graphene quantum dots as a multifunctional nanocomposite. Applied nanoscience. 2021;11(3):849-60.
11. Saladino GM, Kakadiya R, Ansari SR, Teleki A, Toprak MS. Magnetoresponsive fluorescent core-shell nanoclusters for biomedical applications. Nanoscale Adv. 2023;5(5):1323-30.
12. Alaghmandfard A, Sedighi O, Tabatabaei Rezaei N, Abedini AA, Malek Khachatourian A, Toprak MS, et al. Recent advances in the modification of carbon-based quantum dots for biomedical applications. Materials Science and Engineering: C. 2021;120:111756.
13. Shen J, Zhu Y, Yang X, Li C. Graphene quantum dots: emergent nanolights for bioimaging, sensors, catalysis and photovoltaic devices. Chemical Communications. 2012;48(31):3686.
14. Li K, Liu W, Ni Y, Li D, Lin D, Su Z, et al. Technical synthesis and biomedical applications of graphene quantum dots. Journal of Materials Chemistry B. 2017;5(25):4811-26.
15. Choi Y, Thongsai N, Chae A, Jo S, Kang EB, Paoprasert P, et al. Microwave-assisted synthesis of luminescent and biocompatible lysine-based carbon quantum dots. Journal of Industrial and Engineering Chemistry. 2017;47:329-35.
16. Li Q, Zhang S, Dai L, Li L-s. Nitrogen-Doped Colloidal Graphene Quantum Dots and Their Size-Dependent Electrocatalytic Activity for the Oxygen Reduction Reaction. Journal of the American Chemical Society. 2012;134(46):18932-5.
17. Peng J, Gao W, Gupta BK, Liu Z, Romero-Aburto R, Ge L, et al. Graphene Quantum Dots Derived from Carbon Fibers. Nano Letters. 2012;12(2):844-9.
18. Fan L, Hu Y, Wang X, Zhang L, Li F, Han D, et al. Fluorescence resonance energy transfer quenching at the surface of graphene quantum dots for ultrasensitive detection of TNT. Talanta. 2012;101:192-7.
19. Ghasedi A, Koushki E, Baedi J. Cation–π aggregation-induced white emission of moisture-resistant carbon quantum dots: a comprehensive spectroscopic study. Physical Chemistry Chemical Physics. 2022;24(38):23802-16.
20. Liu R, Wu D, Feng X, Müllen K. Bottom-Up Fabrication of Photoluminescent Graphene Quantum Dots with Uniform Morphology. Journal of the American Chemical Society. 2011;133(39):15221-3.
21. Pan D, Zhang J, Li Z, Wu C, Yan X, Wu M. Observation of pH-, solvent-, spin-, and excitation-dependent blue photoluminescence from carbon nanoparticles. Chemical Communications. 2010;46(21):3681.
22. Pan D, Zhang J, Li Z, Wu M. Hydrothermal Route for Cutting Graphene Sheets into Blue-Luminescent Graphene Quantum Dots. Advanced Materials. 2010;22(6):734-8.
23. Li L-L, Ji J, Fei R, Wang C-Z, Lu Q, Zhang J-R, et al. A Facile Microwave Avenue to Electrochemiluminescent Two-Color Graphene Quantum Dots. Advanced Functional Materials. 2012;22(14):2971-9.
24. Tetsuka H, Asahi R, Nagoya A, Okamoto K, Tajima I, Ohta R, et al. Optically Tunable Amino-Functionalized Graphene Quantum Dots. Advanced Materials. 2012;24(39):5333-8.
25. Fan Z, Li Y, Li X, Fan L, Zhou S, Fang D, et al. Surrounding media sensitive photoluminescence of boron-doped graphene quantum dots for highly fluorescent dyed crystals, chemical sensing and bioimaging. Carbon. 2014;70:149-56.
26. Yoon H, Chang YH, Song SH, Lee E-S, Jin SH, Park C, et al. Intrinsic Photoluminescence Emission from Subdomained Graphene Quantum Dots. Advanced Materials. 2016;28(26):5255-61.
27. Sreeprasad TS, Berry V. How Do the Electrical Properties of Graphene Change with its Functionalization? Small. 2012;9(3):341-50.
28. Tetsuka H, Nagoya A, Fukusumi T, Matsui T. Molecularly Designed, Nitrogen-Functionalized Graphene Quantum Dots for Optoelectronic Devices. Advanced Materials. 2016;28(23):4632-8.
29. Qian Z, Ma J, Shan X, Shao L, Zhou J, Chen J, et al. Surface functionalization of graphene quantum dots with small organic molecules from photoluminescence modulation to bioimaging applications: an experimental and theoretical investigation. RSC Advances. 2013;3(34):14571.
30. Sahebalzamani H, Mehrani K, Hosseini HRM, Zare K. Effect of Cysteine Substitutions on the Structural and Magnetic Properties of Fe3O4–Cysteine/RGO and Fe3O4/RGO–Cysteine Nanocomposites. Journal of Superconductivity and Novel Magnetism. 2018;32(5):1299-306.
31. Ahmadi R, Gu N, Madaah Hosseini HR. Characterization of Cysteine Coated Magnetite Nanoparticles as MRI Contrast Agent. Nano-Micro Letters. 2012;4(3):180-3.
32. Bagbi Y, Sarswat A, Mohan D, Pandey A, Solanki PR. Lead and Chromium Adsorption from Water using L-Cysteine Functionalized Magnetite (Fe(3)O(4)) Nanoparticles. Scientific reports. 2017;7(1):7672-.
33. Zhao R, Xiang J, Wang B, Chen L, Tan S. Recent Advances in the Development of Noble Metal NPs for Cancer Therapy. Bioinorg Chem Appl. 2022;2022:2444516-.
34. Dong Y, Shao J, Chen C, Li H, Wang R, Chi Y, et al. Blue luminescent graphene quantum dots and graphene oxide prepared by tuning the carbonization degree of citric acid. Carbon. 2012;50(12):4738-43.
35. Nazari N, Dehghani Mohammad Abadi M, Malek Khachatourian A, Golmohammad M, Nemati A. The effect of phosphorus and nitrogen dopants on structural, microstructural, and

electrochemical characteristics of 3D reduced graphene oxide as an efficient supercapacitor electrode material. Diamond and Related Materials. 2023;137:110144.
36. Tam TV, Hong SH, Choi WM. Facile synthesis of cysteine–functionalized graphene quantum dots for a fluorescence probe for mercury ions. RSC Advances. 2015;5(118):97598-603.
37. Mondal MK, Mukherjee S, Joardar N, Roy D, Chowdhury P, Sinha Babu SP. Synthesis of smart graphene quantum dots: A benign biomaterial for prominent intracellular imaging and improvement of drug efficacy. Applied Surface Science. 2019;495:143562.
38. Gan Z, Xu H, Hao Y. Mechanism for excitation-dependent photoluminescence from graphene quantum dots and other graphene oxide derivates: consensus, debates and challenges. Nanoscale. 2016;8(15):7794-807.
39. Jun SC. Fundamental of Graphene. Graphene-based Energy Devices: Wiley-VCH Verlag GmbH & Co. KGaA; 2015. p. 1-48.
40. Abasali karaj abad Z, Nemati A, Malek Khachatourian A, Golmohammad M. Synthesis and characterization of rGO/Fe2O3 nanocomposite as an efficient supercapacitor electrode material. Journal of Materials Science: Materials in Electronics. 2020;31(17):14998-5005.
41. Abdi Z, Malek Khachatourian A, Nemati A. Visible-light-driven photocatalytic activity of NiFe2O4@Ti-doped ZnO magnetically separable nanoparticles anchored on N-doped rGO nanosheets. Diamond and Related Materials. 2023;135:109839.